In vitro corrosion resistance and *in vivo* osseointegration testing of new multifunctional beta-type quaternary TiMoZrTa alloys

Lucia Carmen Trincă[1], Daniel Mareci[2,†], Carmen Solcan[3,*], Mircea Fântânariu[4], Liviu Burtan[4], Vasile Vulpe[4], Luminița-Diana Hrițcu[4], Ricardo Manuel Souto[5,6,*]

[1] "Ion Ionescu de la Brad" University of Agricultural Science and Veterinary Medicine, Exact Sciences Department, 700490 Iasi, Romania

[2] "Gheorghe Asachi" Technical University of Iasi, Department of Chemical Engineering, 700050 Iasi, Romania

[3] "Ion Ionescu de la Brad" University of Agricultural Science and Veterinary Medicine, Preclinics Department, 700489 Iasi, Romania,

[4] "Ion Ionescu de la Brad" University of Agricultural Science and Veterinary Medicine, Clinics Department, 700489 Iasi, Romania

[5] Department of Chemistry, Universidad de La Laguna, Avda. Astrofísico Sánchez s/n, 38205 La Laguna, Tenerife (Canary Islands), Spain

[6] Instituto Universitario de Materiales y Nanotecnologías, Universidad de La Laguna, P.O. Box 456, 38200 La Laguna, Tenerife (Canary Islands), Spain

Abstract

The present study explores the *in vitro* and *in vivo* responses of new multifunctional quaternary beta-type TiMoZrTa alloys designed for biomedical implantation. The electrochemical resistance to corrosion of the alloys was investigated *in vitro*, using linear potentiodynamic polarization (LPP) and electrochemical impedance spectroscopy (EIS) tests in acidified physiological saline solution at 37 ^{o}C. The pH was adjusted to 4.0 by adding lactic acid in order to simulate the hypoxia stress condition that may occur in the healing process of fractures. The biomaterial alloys spontaneously formed a passivation oxide film on their surfaces, which remained stable for polarizations up to +1.0 V_{SCE}, and became more resistant with the increased amount of Ta in the alloy composition. The animal tests of the quaternary Ti-20Mo-7Zr-*x*Ta alloys showed adequate biocompatibility as a tibial implant. Among them, the 15% Ta-alloy implant showed the best osseointegration according to the results of the biochemical, histological and computed tomography characterizations, and can be considered as a potential biomaterial with low elastic modulus (43.6 GPa).

Keywords: multifunctional beta-type TiMoZrTa alloys; *in vitro* corrosion resistance; bone implants; *in vivo* animal testing; osseointegration.

1. Introduction

Titanium-based alloys are used for the manufacture of biomedical implants, mainly for bone fixation and replacement, and in dentistry [1-4]. The choice of titanium alloys as implant materials is primarily due to their attractive characteristics, namely, good mechanical properties, high resistance to corrosion and excellent biocompatibility with biological materials. Titanium alloys owe their corrosion resistance to the establishment of passivity, that is, to the formation of a very stable oxide film that naturally develops on the surface both in the air and in aqueous environments [5-8]. Although this layer functions as a physical barrier that greatly hinders the release of metal ions into the surrounding biological tissues, small amounts of metal ions are still released from the metallic material [9-13]. This feature is related to the formation of the oxide layer [14,15], to transient breakdown and reforming events of this film [16-18], and to metal debris [19-21]. In addition, acidification is considered detrimental to the stability of the passive regime responsible for corrosion resistance [14].

The biocompatibility performance of a Ti-based alloy is closely related to its corrosion resistance [4,22-24], and the scientific community is making efforts to optimize the composition of the alloy [25-36], modify the surface properties [37-44], and replace the alloying elements that induce adverse physiological reactions [45,46]. In the search for the development of new Ti alloys with optimized corrosion resistance and biocompatibility, the β-stabilizing elements are multifunctional candidates with a low elastic modulus closer to that of the human bone, high strength and good corrosion resistance that they may ensure convenient biocompatibility and osseointegration [47-50]. Recently, improved plasticity and strength have been reported for the quaternary alloys Ti-35Nb-2Ta-3Zr [51] and Ti-24Nb-4Zr-8Sn (Ti2448) [52] compared to the widely used Ti-6Al-4V implant alloy. Thus, the elastic moduli of Ti-35Nb-2Ta [51] and Ti-24Nb-4Zr-8Sn [52] are 48 and ~45 GPa, respectively, which are therefore much lower than that of Ti-6Al-4V (110 GPa [53]) and closer to that of cortical bone (30 GPa [1]). In addition, these materials exhibit optimized corrosion resistance and better biocompatibility and osseointegration than Ti-6Al-4V [54-58].

More recently, our group also found promising results for Ti-15Mo-7Zr-15Ta in Ringer's physiological solution based on electrochemical characterization [59] while presenting a low elastic modulus (52 GPa) [60] and a pronounced hydrophilic character [61]. Microstructural characterization of this alloy showed β-phase to be the main component [59], therefore demonstrating that stabilization of the β-phase was satisfactorily achieved by adding Mo, Zr and Ta to titanium. The 15 wt.% Mo content was chosen to match the amount

approved for the manufacture of binary β-Ti alloy implant devices in norm ASTM F 2066 [62]. On the other hand, an investigation on the effects of Mo content in binary TiMo alloys demonstrated that contents higher than 15 wt.% exhibited greater corrosion resistance and the formation of a more compact inner oxide layer for enhanced passivity [63].

This work reports a study of the electrochemical behavior of three Ti-20Mo-7Zr-*x*Ta (*x* = 5, 10, 15 wt.%) alloys with "molybdenum equivalent" ([Mo_{eq}], [64]) around 20 [65], enough to stabilize the β phase (bcc) in the alloy [66]. The rationale for the variation of the tantalum content in the alloys was to explore the potential beneficial effect of this element in bone surgery, because it has been shown that tantalum alloys can activate the functionality of osteoblasts and matrix mineralization (that is, promoting osseointegration and bone ingrowth) [67,68]. Since acidification is considered detrimental to the passive regime of the biomaterial [15], as well as to the normal fracture repairing process [69], the first objective of this study was to test *in vitro* the corrosion resistance of the Ti-20Mo-7Zr-*x*Ta alloys in physiological saline solution acidified at 4.0 pH value, at 37 ^{o}C. Such acidification was produced by the addition of lactic acid, to simulate the existing stress condition under systemic or local acidosis induced by hypoxia (through reduced perfusion and increased anaerobic metabolism), which is capable of generating inflammation and can subsequently affect the normal healing of fractures and wounds if persisting for a sufficiently long time [70]. The resistance to corrosion was characterized by electrochemical tests, using linear potentiodynamic polarization (LPP) and electrochemical impedance spectroscopy (EIS). The second objective was to evaluate *in vivo* the biocompatibility and degradation behavior of the quaternary TiMoZrTa alloys by carrying out biochemical, histological and computed tomography investigations.

2. Materials and Methods

2.1. Materials and material characterization

Three quaternary TiMoZrTa alloys have been synthesized by electron beam melting method as described in reference [60]. The melting procedure was repeated three times in order to obtain the chemically homogenized alloys. Their chemical compositions were determined by EDX analysis. A Quanta 200 scanning electron microscope (FEI, Hillsboro, OR, USA), operated at an accelerating voltage of 30 kV, and equipped with EDX detector, was employed for this purpose. The chemical compositions (wt.%) and "molybdenum equivalent" [Mo_{eq}] [64] of the quaternary TiMoZrTa alloys are given in Table 1.

2.2. Electrochemical characterization

Modified Fusayama physiological solution was used as the electrochemical test electrolyte. It consisted of 0.400 g NaCl, 0.400 g KCl, 0.795 g $CaCl_2 \cdot 2H_2O$, 0.780 g $NaH_2PO_4 \cdot 2H_2O$, 0.005 g $Na_2S \cdot 9H_2O$, 1.000 g NH_2CONH_2, and distilled water up to 1000 mL. The pH of this solution was lowered down to 4.0 by adding lactic acid. The pH was measured with a CONSORT 831C multiparameter analyser (Turnhout, Belgium). The temperature of the simulated physiological environment was maintained at 37 ± 1 ^{o}C throughout *in vitro* tests.

The electrochemical measurements were conducted with a potentiostat model PARSTAT 4000 (Princeton Applied Research (PAR), Princeton, NJ, USA). A glass corrosion cell kit (C145/170, Radiometer, France) was employed. A sample of the TiMoZrTa alloy was connected as the working electrode, a platinum gauze as the auxiliary electrode, and a saturated calomel electrode (SCE) as the reference. All potential values reported herein are expressed with respect to SCE. The instrument was controlled by a personal computer and *Versa Studio software*®.

Electrochemical impedance spectra (EIS) were recorded in the 10^{-2} Hz to 10^{5} Hz frequency range applying an alternating potential signal of 0.010 V amplitude. In order to enable quantitative analysis of EIS data, an appropriate model for equivalent circuit (EC) quantification with *ZSimpWin*® software was used. Impedance spectra were recorded at various times up to 7 days of the alloys exposed to the simulated physiological solution.

After 7 days exposure, linear potentiodynamic polarization (LPP) tests were initiated. First, Tafel measurements were performed from the open circuit potential (E_{OC}) down to (E_{OC} – 0.10) V, and then from E_{OC} up to (E_{OC} + 0.10) V, at the rate of 1×10^{-3} V s^{-1}. From these measurements, the zero current potential (ZCP), corrosion current density (j_{corr}), and Tafel slopes (-βc and βa, for the cathodic and the anodic branches, respectively) were determined. Next, potentiodynamic curves were recorded by scanning the potential, at the rate of 1×10^{-3} V s^{-1}, from -1.0 V_{SCE} up to +1.0 V_{SCE}. The passive current density (j_{pass}) was determined from these plots. *PowerCorr*® software was employed both to conduct the electrochemical operation and to determine corrosion parameters.

After completing the electrochemical tests, TiMoZrTa samples were retrieved for SEM observation and EDX quantification in order to determine any surface changes produced by the electrochemical polarization.

2.3. Animal testing

A total of 20 Sprague–Dawley rats, 8 weeks of age, with 200–220 g average body weight, were employed for the *in vivo* evaluation of 1 month duration. The rats were hosted in individual cages, with free water and food access, in Iaşi Agronomical and Veterinary Medicine University's Biobase according ISO 10993-2:2006 animal welfare requirements [71]. The 20 animals were equally distributed into four groups. The control group consisted of rats with no implants. Cylindrical shape alloy samples (3 mm diameter x 4 mm length) were implanted as follows: Ti-20Mo-7Zr-5Ta alloy in rats from G_1 group, Ti-20Mo-7Zr-15Ta alloy in rats from G_2 group, and pure titanium (Cp-Ti) in rats from G_3 group (positive control). The implantation procedure has been described elsewhere [72], and it was performed with the agreement supervision of the Iasi Veterinary Medicine Faculty's Ethics Committee. After anesthesia, skin incision and tibial crest exposition, a circular orifice (4 mm diameter) was made using stainless steel intramedullary pin drill (see Figure 1). After implantation, daily clinical observation was performed.

2.4. Biochemical analysis

Blood samples were collected by cardiac puncture under anesthetic condition in the 14^{th} and 28^{th} days post implantation. Calcium, inorganic phosphate, alkaline phospatase (ALKP) and total proteins (TP) were determined in blood serum with a BS-130 Auto Chemistry automatic analyzer (Golden Harvest Industries, Nagar, Chennai, Tamil Nadu, India) by using specific kit tests. The results were statistically processed by using unpaired Student test, with $p < 0.05$ statistically significant.

2.5. Histological analysis

The preliminary processing of histological samples was described elsewhere [73]. Thick coronal sections (5-6 μm) of the callus central area, from the defect site, were stained with hematoxylin-eosin (HE method) and with periodic acid–Schiff (PAS method) according to the general procedure for histological investigations [74]. The stained sections were microscopically evaluated by light microscopy with 100-1000× magnifications.

2.6. Computed tomography analysis

X-ray computed tomography was performed with a Siemens Somatom Balance CT scanner (Erlangen, Germany) on rats of each group that were previously anesthetized using 4

mg Xylazine + 100 mg Ketamine, given by intramuscular injection. 3D and 2D -images were processed with *2.21 Syngo fastView* software.

3. Results

3.1. Electrochemical characterization

In order to obtain information about the characteristics of the electrochemical processes that occur at the interface between the TiMoZrTa alloys and the acidified physiological solution, electrochemical impedance spectroscopy (EIS) tests were performed at different immersion times in the test solution ranging from 1 hour to 7 days. Figure 2 shows the recorded impedance spectra in the form of Nyquist (complex versus real components of the impedance; A,C,E) and Bode (impedance modulus and phase angle versus frequency diagrams; B,D,F) diagrams. The Nyquist diagrams display two depressed pseudo-capacitive semicircles at all times. The high-frequency semicircle can be related to the double electrochemical layer developed on the surface of the metallic material, while the low-frequency semicircle can be associated with the passive layer formed on the surface of the alloys. Therefore, an increase in the diameter of the semicircle correlates with a decrease in the corrosion rate of the material. Over time, the tendency of change in the Nyquist plots evidenced that the corrosion resistance of all TiMoZrTa alloys increased.

The electrochemical behavior of the three alloys was further investigated using linear potentiodynamic polarization techniques. First, semi-logarithmic plots were recorded between -1.0 and +1.0 V_{SCE} after immersing the samples for 7 days in the simulated physiological solution at 37 ^{o}C. Figure 3 depicts typical polarization curves for the three TiMoZrTa alloys. The values of the zero current potential (ZCP) and the corrosion current (j_{cor}) were determined by Tafel analysis of the anodic and cathodic branches of the polarization plots, as shown in the inset provided in Figure 3. The ZCP is defined as the potential at which the current reaches a minimum during the forward potentiodynamic polarization scan. The corrosion current is representative of the degree of degradation of each sample. The average ZCP and j_{cor} values determined from the polarization curves measured for at least 3 samples for each alloy are presented in Table 2.

The samples were recovered at +1.0 V_{SCE} after completing the electrochemical tests in the acidified simulated physiological solution, and they were subjected to surface morphology and composition analysis to evaluate the combined effect of the environment and electric

polarization in the samples. Figure 4 shows characteristic SEM micrographs and EDX observation of the retrieved TiMoZrTa samples.

3.2. Biochemical characterization

The main blood biochemical markers in rats with tibial implants were determined at 14 and 28 days after implantation. Similar tests were performed for the rats in the control group, that is, without implantation. Table 3 lists calcium (Ca), inorganic phosphate, alkaline phosphatase (ALKP) and total proteins (TP) determined from blood serum for control and experimental groups.

The serum calcium ion concentration at 2 weeks after implantation showed a decrease in all groups compared to the values of the normal group. There were statistically significant hypocalcemiae decreases ($p < 0.05$; $n = 5$) in the case of the G3 group, with pure titanium implant, as well as in the case of G1 and G2 groups, with quaternary TiMoZrTa alloys implants. But statistically insignificant variations ($p > 0.05$; $n = 5$) were found when the experimental groups were compared between them. In the 28th day after implantation, the value of the serum calcium ion concentration was statistically insignificant only in the case of the group G2 (i.e., with the Ti-20Mo-7Zr-15Ta alloy implant) and G3 group (with the pure titanium implant, Cp-Ti) as compared with the normal group. The reduction of the serum calcium ion variations by approaching the normal values is induced by osteoclast activation that will strengthen the recovery of the bone tissue recovery in the later stages of remodeling [75].

The values of the inorganic phosphate concentration in serum showed different modes of variation in the experimental groups compared to the control group. Thus, in the case of the G3 group with pure titanium implant (positive control), group G1 (with Ti-20Mo-7Zr-5Ta alloy implant) and group G2 (with Ti-20Mo-7Zr-15Ta alloy implant), significant hypophosphatemia ($p <0.05$; $n = 5$) was recorded at 2 weeks after implantation. After 4 weeks implantation, the serum inorganic phosphate approached the normal values only in the case of the G2 group (with Ti-20Mo-7Zr-15Ta alloy implant). These variations confirm the ability of inorganic phosphate to function as a specific biomarker by highlighting the main stages repair of bone fractures [76,77].

Finally, the activity values of ALKP in relation to the total protein content at 2 weeks after implantation showed an increase in the experimental groups. In the case of group G3 with Cp-Ti implant (positive control), a slight insignificant increase was registered at the 14th day post implantation. Conversely, both experimental groups with quaternary TiMoZrTa alloy

implants showed greater increases, statistically more significant ($p < 0.05$; $n = 5$) in the case of group G2 (Ti-20Mo-7Zr-15Ta alloy implant) than for group G1(Ti-20Mo-7Zr-5Ta alloy implant). The observed decreasing trend of the alkaline phosphatase activity at the 28th day (as compared with the 14th day after implantation) was highly statistically significant ($p < 0.001$; $n = 5$) in the case of group G2 (Ti-20Mo-7Zr-15Ta alloy implant), very statistically significant ($p < 0.01$; $n = 5$) for the group G1 (Ti-20Mo-7Zr-5Ta alloy implant), and significant ($p <0.05$; $n = 5$) in the case of the group G3 (Cp-Ti implant). This fact evidences a normal evolution of the bone fracture with a resorption stage at the background of a relatively constant bone formation rate, which is controlled by the transformation of the osteoblasts into osteocytes, and the subsequent activation of the osteoclasts [78-80].

3.3. Histomorphometry characterization

Figures 5-7 show representative images of the histological investigation of the osseous tissue of rats with tibial implants after either 14 or 28 days of healing. In the case of the G1 group, which consists of rats with Ti-20Mo-7Zr-5Ta alloy implant, peripheral-induced ongoing repairing phenomena are observed on the 14th day implantation (see Figure 5A-B). The image shows numerous macrophages with phagocytized wear pigments staining brown, which are oriented to surround the old bony necrotic areas (staining dark purple). On day 28 after implantation, the images in Figures 5C-D show the newly formed osteoid tissue surrounded by a fibrous background, the osteoblasts lining the spicules of woven bone, and a few osteocytes in lacunae (with higher staining affinity).

Similarly, Figure 6A-B shows the biological response for the group G2 (with the Ti-20Mo-7Zr-5Ta alloy implant) on the 14th day after implantation. Areas of bone necrosis (stained dark violet) are surrounded by numerous macrophages loaded with phagocytized wear pigments (stained brown). The inflammatory reaction determined the aggregation of the fibrous connective tissue that contains mono- and polymorphonuclear inflammatory infiltrate. In the bone tissue, nearby the implant, large trabeculae containing a fairly small amounts of osteoblasts are evident. The presence of some apoptotic osteocytes can already be noticed inside the lacunae. On day 28 after implantation, Figure 6C presents the appearance of the new bone tissue with a roughened rock-like surface, while Figure 6D highlights the mini-remodeling of the new osseous matrix with two different origins, namely, the areas of less intense color represent the osseous matrix secreted by the osteoblasts adjacent to the bay bone, while the areas of more intense color areas are cartilage matrices containing type II collagen and chondroitin sulphate glycoproteins.

In the case of group G3 with Cp-Ti implant (positive control), on the 14th day after implantation, red blood cells from bone marrow surrounding the necrotic bone area can be observed (see Figure 7A-B). The images recorded at day 28 after implantation given in Figure 7C-D, show numerous osteoblasts that synthesize the collagen matrix I (lighter colored areas), whereas the old mature bone is represented by the darker colored areas. The onset of bone mini-remodeling phenomena is evidenced by the simultaneous observation of osteoclasts and nucleated osteocytes.

3.4. Tomography characterization

Computed tomography (CT) allows a non-invasive and accurate evaluation of the process of biodegradation of the implant [81], highlighting at the same time the main stages of the fracture recovery process [82,83]. Figure 8 presents 3D and 2D reconstructed images of CT investigations performed on rats from each experimental group. Regarding the *in vivo* biodegradability/corrosion of the implants tested, the structural integrity of the implant was preserved significantly in the case of the Ti-20Mo-7Zr-15Ta alloy implant, as evidenced by the intensity of the blue coloration in Figure 8B as a proportional measure of the hardness of the biomaterial hardness. On the other hand, the Ti-20Mo-7Zr-5Ta alloy implant in Figure 8A showed a significant deterioration of the structure compared to the control of the cp-Ti implant (cf. Figure 8C). In addition, Figure 8B also shows that there was an increase in the area with the blue color and in the color intensity related to the tibial bone tissue (i.e., highlighting both the activation of the osteoblasts activation and mineralization of the matrix) in the case of the Ti-20Mo-7Zr-15Ta alloy implant. This fact evidences that a higher content of Ta in the alloy can ensure a better promotion of osseointegration and bone ingrowth.

4. Discussion

4.1. In vitro corrosion resistance testing

The corrosion resistance of quaternary TiMoZrTa alloys was investigated on the basis of the electrochemical tests carried out for these materials during the immersion in acidified simulated physiological solution at 37 ºC. The electrochemical impedance spectra exhibit two time constants at all elapsed times, one corresponding to the thin native oxide film, and the other to the charge transfer process that occurs at the surface of the alloys. Therefore, the corrosion resistance of the TiMoZrTa alloys was due to the formation of a protective

passivating oxide layer. The stronger the passive layer is, the greater the resistance to corrosion achieved by the underlying metal.

Quantitative data to assist in the interpretation of EIS results can be obtained by using an electrical analog that represents the physicochemical processes occurring on the surface of the alloys. This is achieved by fitting an equivalent circuit (EC) to the experimental EIS data. The best fit between the calculated and experimental data was obtained using the equivalent circuit depicted in Figure 9. This EC describes a two-layer oxide film, consisting of an unsealed outer porous layer and a compact inner layer [5]. The resistance to corrosion conferred by the passive layer formed on the metal arises mainly from the compact inner layer that acts as a physical barrier that prevents direct contact between the metal and the species contained in the solution phase. The model consisted of R_{sol} (solution resistance) associated in series to the two parallel constant phase element/resistor pairs, Q_1/R_1 and Q_2/R_2, where the subscripts 1 and 2 designate the time constants found in the ranges of low and high frequency, respectively. The parameters R_2/Q_2 corresponds to the barrier characteristics of the oxide film towards electrolyte penetration that dominates the impedance response in the low frequency range, while R_1/Q_1 are the parameters related to the charge transfer process at the surface of the alloys (i.e., the actual corrosion process). The impedance values extracted from the spectra in the medium to low frequency ranges for the three quaternary TiMoZrTa alloys at their open circuit potential, indicated large polarization resistances for these systems (cf. Table 4). This feature is consistent with the two-layer model of a surface film with two time constants under consideration.

The use of a constant phase element (CPE, Q) was required due to the occurrence of a non-ideal distributed relaxation characteristic, which is observed as a depressed semicircle in the Nyquist plots. This distributed parameter in the EC contains a non-integral power dependency in the frequency [84]. The impedance of the CPE element is given by:

$$Z_{CPE} = \frac{1}{Q(j\omega)^n} \quad (1)$$

where Q is the magnitude of the CPE, ω the angular frequency, j the imaginary complex number $(-1)^{1/2}$, and the n value indicates the nature of the element (n = 0 corresponds to a resistor, and n = 1 means that the CPE behaves as a pure capacitor). The values were always greater than 0.8, which can indicate passive layers with a rather smooth surface.

The presence of a protective passive layer provided the high corrosion resistance of these TiMoZrTa alloys in acidified artificial saliva solution at pH = 3.5. Indeed, the contribution of the charge transfer resistance in the impedance data is considered almost

negligible for all TiMoZrTa alloys. Furthermore, it can be observed in Table 4 that the value of the passive layer resistance obtained at open circuit potential, R_2, increases with [Mo_{eq}]. This fact demonstrates that the passive layer formed spontaneously in TiMoZrTa alloys becomes more resistant when the amount of Ta in the quaternary alloy increases. In summary, EIS analysis leads to the observation that the corrosion resistance of Ti-based alloys immersed in acidified artificial saliva was improved with the addition of β-stabilizing elements. It is concluded that the additions of the β-stabilizing elements had a positive contribution to the formation of the passive oxide film.

Low corrosion current density values were obtained from the potentiodynamic polarization curves (LPP) for all the samples investigated in the acidified simulated physiological environment. The anodic polarization curves exhibited a typical passive region up to +1.0 V_{SCE} for all TiMoZrTa alloys, a more positive value than the highest recorded in the human body so far [85]. Therefore, the high alloying addition of tantalum, which increase [Mo_{eq}] to TiMoZrTa alloys, has been clearly shown to reduce the dissolution rate of TiMoZrTa alloys.

The electrochemical characterization findings are supported by the SEM images of the samples recovered from the *in vitro* tests, since they show a fairly uniform topography for all the samples, while the chemical analysis indicates the occurrence of a uniform oxidation process in the surface. No evidence of passive layer breakdown and propagation was found in any of the samples investigated.

4.2. In vivo osseointegration testing

In summary, our *in vivo* investigations highlighted an intrinsic link between the metabolic changes, the results of histological analysis and the computer tomography investigations occurring in the bone fracture repairing process as derived from the implantation of cylindrically-shaped samples in the tibiae of Sprague-Dawley rats.

In general, these histological images captured the main recovery stages of principal bone evolution reported in rats [86,87], confirming the multifunctional capacity of Ta to activate the functionality of osteoblasts and the mineralization of the osseous matrix in order to promote osseointegration compared to pure titanium. These observations were also confirmed by computed tomography, with the Ti-20Mo-7Zr-15Ta alloy implant exhibiting the highest osteoblast activation as well as the matrix mineralization. In addition, analysis of blood serum at 2 and 4 weeks of implantation indicated a good rate of bone formation with a

faster acquisition of biomarkers values closer to control non-implanted animals in the case of the individuals implanted with the Ti-20Mo-7Zr-15Ta alloy.

4.3. Concluding remarks

Previous reports focused on the microstructure and mechanical properties of quaternary TiMoZrTa alloys with [Mo_{eq}] around 20, and showed that these materials exhibit very attractive properties to be considered potential candidates for implant applications. Namely, they present the elasticity modulus values closest to the human bone reported thus far (namely, 43.6 GPa for Ti-Mo-7Zr-15Ta) while increasing mechanical strength (e.g., hardness 397.56 HV and stiffness 3.20 N μm^{-1}) [60]. Secondly, the addition of Mo and Ta contributed greatly to stabilize the β phase, while the eventual formation of the α phase could not be detected from XRD data [59]. Thirdly, thermal analysis showed stable behavior within the temperature range a biomaterial works in the human body [61]. And they have a pronounced hydrophilic character indicated by a H_2O contact angles close to 56º [61].

On the other hand, the electrochemical characterization of the TiMoZrTa alloys carried out in this work has shown that they exhibit high resistance to corrosion while immersed in acidified simulated physiological solution at 37 ºC due to the formation of a bilayer passive oxide film at the OCP. Passive films remain stable within the potential range that can be achieved in the human body even in inflammatory and surgical stages. It can be concluded that the additions of the β stabilizing elements had a positive contribution to the formation of the passive oxide film.

In addition, animal testing of TiMoZrTa alloys showed adequate biocompatibility as a tibial implant in rats based on biochemical, histological and computed tomography characterizations. Among them, the 15% Ta-alloy implant showed the best osseointegration and the highest resistance to corrosion.

Therefore, the results obtained in this study of a combined *in vitro* and *in vivo* characterization methodology demonstrate that multifunctional quaternary TiMoZrTa alloys are potential materials for the manufacture of biomedical implants due to their superior corrosion resistance and osseointegration characteristics compared to pure titanium.

5. Conclusions

The development of passivity for the three TiMoZrTa alloys after immersion in an acidified simulated physiological solution with pH = 4.0 was confirmed from electrochemical impedance (EIS) and linear potentiodynamic polarization (LPP) measurements. The EIS results show that the passive oxide film formed in the alloys is rather compact, characteristic for a sealed inner oxide layer that effectively acts as a barrier film towards the dissolution of the metal, and an outer more porous and thicker oxy-hydroxide layer. This bilayer film ensures an optimized corrosion resistance to these alloys. The LPP results are consistent with the trends observed in the EIS tests.

The addition of Ta in TiMoZrTa at high Ta contents (15 wt.%) induces the formation of a more compact oxide layer. This study demonstrated the importance of the different [Mo_{eq}] contents in the resistance to corrosion and the electrochemical behavior of TiMoZrTa alloys.

The Ti-20Mo-7Zr-15Ta alloy presented a very good biocompatibility as tibial implant according to the results of biochemical, histological and computed tomography investigations compared to pure titanium. Enhanced bone formation was observed, leading to improved integration in rat tibia.

Acknowledgements

The authors would like to thank Professor Victor Geantă (University Politehnica of Bucharest, Romania), for providing the TiMoZrTa alloys used in this investigation. This work was supported partially by the Romanian National Authority for Scientific Research (CNCS-UEFISCDI, project No. PN-II-IDPCE-2011-3-0218), and by the Spanish Ministry of Economy and Competitiveness (MINECO, Madrid, Spain) and the European Regional Development Fund (project No. CTQ2016-80522-P).

References

1. D.F. Williams, Biocompatibility of clinical implant materials, in: Biocompatibility of clinical impact materials, vol. 1, D.F. Williams (Ed.); CRC Press, Boca Raton, FL, 1981, p. 9.
2. P. Kovacs, J.A. Davidson, Chemical and electrochemical aspects of the biocompatibility of titanium and its alloys, in: S.A. Brown, J.E. Lemons (Eds.), Medical Applications of Titanium and its Alloys: The Materials and Biological Issues, American Society for Testing and Materials, West Conshohocken, PA, 1996, p. 163.
3. M. Geetha, A.K. Singh, R. Asokamani, A.K. Gogia, Ti based biomaterials, the ultimate choice for orthopaedic implants – A review, Prog. Mater. Sci. 54 (2009) 397-425.

4. M. Niinomi, M. Nakai, J. Hieda, Development of new metallic alloys for biomedical applications, Acta Biomater. 8 (2012) 3888-3903.
5. J. Pan, D. Thierry, C. Leygraf, Electrochemical impedance spectroscopy study of the passive oxide film on titanium for implant application, Electrochim. Acta 41 (1996) 1143-1153.
6. J. Pan, H. Liao, C. Leygraf, D. Thierry, J. Li, Variation of oxide films on titanium induced by osteoblast-like cell culture, and influence of an H_2O_2 pretreatment, J. Biomed. Mater. Res. 40 (1998) 244-256.
7. I. Milosev, T. Kosec, H.H. Strehblow, XPS and EIS study of the passive film formed on orthopaedic Ti-6Al-7Nb in Hank's physiological solution, Electrochim. Acta 53 (2008) 3547-3558.
8. J.C. Mirza Rosca, E. Vasilescu, P. Drob, C. Vasilescu, S.I. Drob, Corrosion behaviour in physiological fluids of surface films formed on titanium alloys, Mater. Corros. 63 (2012) 527-533.
9. I. Milošev, V. Antolič, A. Minovič, A. Cör, S. Herman, V. Pavlovčič, P. Campbell, Extensive metallosis and necrosis in failed prostheses with cemented titanium-alloy stems and ceramic heads, J. Bone Joint Surg. 82B (2000) 352-357.
10. S. Ichinose, T. Muneta, I. Sekiya, S. Itoh, H. Aoki, M. Tagami, The study of metal ion release and cytotoxicity in Co-Cr-Mo and Ti-Al-V alloy in total knee prosthesis, J. Mater. Sci. 14 (2003) 79-86.
11. Y. Okazaki, E. Gotoh, Comparison of metal release from various metallic biomaterials in vitro, Biomaterials 26 (2005) 11–21.
12. Y. Nuevo-Ordóñez, M. Montes-Bayón, E. Blanco-González, J. Paz-Aparicio, J.D. Raimundez, J.M. Tejerina, M.A. Peña, A. Sanz-Medel, Titanium release in serum of patients with different bone fixation implants and its interaction with serum biomolecules at physiological levels, Anal. Bioanal. Chem. 401 (2011) 2747-2754.
13. O. Addison, A.J. Davenport, R.J. Newport, S. Kalra, J.W.F. Mosselmans, D. Proops, R.A. Martin, Do "passive" medical titanium surfaces deteriorate in service in the absence of wear?, J. Royal Soc. Interface 9 (2012) 3161-3164.
14. P. Ducheyne, G. Willems, M. Martens, J. Helsen, Invivo metal-ion release from porous titanium-fiber material, J. Biomed. Mater. Res. 18 (1984) 293-308.
15. K.E. Healy, P. Ducheyne, The mechanisms of passive dissolution of titanium in a model physiological environment, J. Biomed. Mater. Res. 26 (1992) 319-338.

16. G.T. Burstein, R.M. Souto, Observations of localised instability of passive titanium in chloride solution, Electrochim. Acta 40 (1995) 1881-1888.
17. R.M. Souto, G.T. Burstein, A preliminary investigation into the microscopic depassivation of passive titanium implant materials *in vitro*, J. Mater. Sci.: Mater. Med. 7 (1996) 337-343.
18. G.T. Burstein, C. Liu, R.M. Souto, The effect of temperature on the nucleation of corrosion pits on titanium in Ringer's physiological solution, Biomaterials 26 (2005) 245-256.
19. C.P. Case, V.G. Langkamer, C. Jamec, M.R. Palmer, A.J. Kemp, P.F. Heap, L. Solomon, Widespread dissemination of metal debris from implants, J. Bone Joint Surg. 76B (1994) 701-712.
20. P. Korovessis, G. Petsinis, M. Repanti, T. Repantis, Metallosis after contemporary metal-on-metal total hip arthroplasty. Five to nine-year follow-up, J. Bone Joint Surg. 88A (2006) 1183-1191.
21. L. Mohan, C. Anandan, Wear and corrosion behavior of oxygen implanted biomedical titanium alloy Ti–13Nb–13Zr, Appl. Surf. Sci. 282 (2013) 281-290.
22. S. Rao, Y. Okazaki, T. Tateishi, T. Ushida, Y. Ito, Cytocompatibility of new Ti alloy without Al and V by evaluating the relative growth ratios of fibroblasts L929 and osteoblasts MC3T3-E1 cells, Materials Science & Engineering C 4 (1997) 311-314.
23. N.J. Hallab, S. Anderson, M. Caicedo, A. Brasher, K. Mikecz, J.J. Jacobs, Effects of soluble metals on human peri-implant cells, J. Biomed. Mater. Res. 74A (2005) 124-140.
24. Q. Mohsen, S.A. Fadl-Allah, Improvement in corrosion resistance of commercial pure titanium for the enhancement of its biocompatibility, Mater. Corros. 62 (2011) 310-319.
25. D. Kuroda, M. Niinomi, M. Morinaga, Y. Kato, T. Yashiro, Design and mechanical properties of new beta type titanium alloys for implants materials, Mater. Sci. Eng. A 243 (1998) 244-249.
26. M. Aziz-Kerrzo, K.G. Conroy, A.M. Fenelon, S.T. Farrell, C.B. Breslin, Electrochemical studies on the stability and corrosion resistance of titanium-based implant materials, Biomaterials 22 (2001) 1531-1539.
27. S.L. Assis, S. Wolynec, I. Costa, The electrochemical behaviour of Ti-13Nb-13Zr alloy in various solutions, Mater. Corros. 59 (2008) 739-743.
28. M. Atapour, A.L. Pilchak, G.S. Frankel, J.C. Williams, Corrosion behavior of β titanium alloys for biomedical applications, Mater. Sci. Eng. C 31 (2011) 885-891.

29. S. Yang, D.C. Zhang, M. Wei, H.X. Su, W. Wu, J.G. Lin, Effects of the Zr and Mo contents on the electrochemical corrosion behavior of Ti–22Nb alloy, Mater. Corros. 64 (2013) 402-407.
30. M. Dilea, A. Mazare, D. Ionita, I. Demetrescu, Comparison between corrosion behaviour of implant alloys Ti6Al7Nb and Ti6Al4Zr in artificial saliva, Mater. Corros. 64 (2013) 493-499.
31. R. Chelariu, G. Bolat, J. Izquierdo, D. Mareci, D.M. Gordin, T. Gloriant, R.M. Souto, Metastable beta Ti-Nb-Mo alloys with improved corrosion resistance in saline solution, Electrochim. Acta 137 (2014) 280-289.
32. Y. Li, C. Yang , H. Zhao, S. Qu, X. Li, Y. Li, New developments of Ti-based alloys for biomedical applications, Materials 7 (2014) 1709-1800.
33. J.M. Calderon Moreno, C. Vasilescu, S.I. Drob, E.I. Neacsu, M. Popa, Evaluation of the microstructural, mechanical and anti-corrosive properties of a new ternary Ti-15Zr-5Nb alloy in simulated oral environment, Mater. Corros. 65 (2014) 703-714.
34. A.C. Bărbînță, D. Mareci, R. Chelariu, G. Bolat, C. Munteanu, K. Cho, M. Niinomi, The estimation of corrosion behavior of new TiNbTaZr alloys for biomedical applications, Mater. Corros. 65 (2014) 1017-1023.
35. H. Liu, M. Niinomi, M. Nakai, K. Cho, β-Type titanium alloys for spinal fixation surgery with high Young's modulus variability and good mechanical properties, Acta Biomater. 24 (2015) 361-369.
36. A. Biesikierski, J. Lin, Y. Li, D. Ping, Y. Yamabe-Mitarai, C. Wen, Impact of ruthenium on mechanical properties, biological response and thermal processing of β-type Ti-Mb-Ru alloys, Acta Biomater. 48 (2017) 461-467.
37. D. Ionita, M. Grecu, C. Ungureanu, I. Demetrescu, Modifying the TiAlZr biomaterial surface with coating, for a better anticorrosive and antibacterial performance, Appl. Surf. Sci. 257 (2011) 9164-9168.
38. N. Harmankaya, K. Igawa, P. Stenlund, A. Palmquist, P. Tengvall, Healing of complement activating Ti implants compared with non-activating Ti in rat tibia, Acta Biomater. 8 (2012) 3532-3540.
39. J. Karlsson, R. Jimbo, H.M. Fathali, H.O. Schwartz-Filho, M. Hayashi, M. Halvarsson, A. Wennerberg, M. Andersson, In vivo biomechanical stability of osseointegrating mesoporous TiO_2 implants, Acta Biomater. 8 (2012) 4438-4446.

40. G. Bolat, J. Izquierdo, J.J. Santana, D. Mareci, R.M. Souto, Electrochemical characterization of ZrTi alloys for biomedical applications. Part 2: The effect of thermal oxidation, Electrochim. Acta 106 (2013) 432–439.
41. J. Li, X. Wang, R. Hu, H. Kou, Structure, composition and morphology of bioactive titanate layer on porous titanium surfaces, Appl. Surf. Sci. 308 (2014) 1-9.
42. T. Wierzchoń, E. Czarnowska, J. Grzonka, A. Sowińska, M. Tarnowski, J. Kamiński, K. Kulikowski, T. Borowski, K.J. Kurzydłowski, Glow discharge assisted oxynitriding process of titanium for medical application, Appl. Surf. Sci. 334 (2015) 74-79.
43. L. Salou, A. Hoornaert, G. Louarn, P. Layrolle, Enhanced osseointegration of titanium implants with nanostructured surfaces: An experimental study in rabbits, Acta Biomater. 11 (2015) 494-502.
44. P. Kwaśniak, J. Pura, M. Zwolińska, P. Wieciński, H. Skarżyński, L. Olszewski, J. Marczak, H. Garbacz, K.J. Kurzydłowski, Laser and chemical surface modifications of titanium grade 2 for medical application, Appl. Surf. Sci. 336 (2015) 267-273.
45. C. Morant, M.F. López, A. Gutiérrez, J.A. Jiménez, AFM and SEM characterization of non-toxic vanadium-free Ti alloys used as biomaterials, Appl. Surf. Sci. 220 (2003) 79-87.
46. T.I. Kim, J.H. Han, I.S. Lee, K.H. Lee, M.C. Shin, B.B. Choi, New titanium alloys for biomaterials: A study of mechanical and corrosion properties and cytotoxicity, Bio-Med. Mater. Eng. 7 (1997) 253-263.
47. M. Long, H.J. Rack, Titanium alloys in total joint replacement—a materials science perspective, Biomaterials 19 (1998) 1621-1639.
48. M. Niinomi, Mechanical properties of biomedical titanium alloys, Mater. Sci. Eng. A 243 (1998) 231-236.
49. G. He, J. Eckert, Q.L. Dai, M.I. Sui, W. Löser, M. Hagiwara, E. Ma, Nanostructured Ti-based multi-component alloys with potential for biomedical applications, Biomaterials 24 (2003) 5115-5120.
50. A. Balamurugan, S. Rajeswari, G. Balossier, A.H.S. Rebelo, J.M.F. Ferreira, Corrosion aspects of metallic implants — An overview, Mater. Corros. 59 (2008) 855-869.
51. L. Wang, W. Lu, J. Qin, F. Zhang, D. Zhang, Microstructure and mechanical properties of cold-rolled TiNbTaZr biomedical β titanium alloy, Mater. Sci. Eng. A 490 (2008) 421-426.

52. Y.L. Hao, S.J. Li, S.Y. Sun, C.Y. Zheng, R. Yang, Elastic deformation behaviour of Ti-24Nb-4Zr-7.9Sn for biomedical applications, Acta Biomater. 3 (2007) 277-286.
53. R. Banerjee, S. Nag, H.L. Fraser, A novel combinatorial approach to the development of beta titanium alloys for orthopaedic implants, Mater Sci Eng C 25 (2005) 282-289.
54. Z. Guo, J. Fu, Y.Q. Zhang, Y.Y. Hu, Z.G. Wu, L. Shi, M. Sha, S.J. Li, Y.L. Hao, R. Yang, Early effect of Ti–24Nb–4Zr–7.9Sn intramedullary nails on fractured bone, Mater Sci Eng C 29 (2009) 963-968.
55. Y. Guo, M. Cheng, D. Chen, X. Xue, X. Zhang, In vitro corrosion resistance and cytotoxicity of novel TiNbTaZr alloy, Trans. Nonferrous Met. Soc. China 22 (2012) s175-s180.
56. Y. Guo, D. Chen, M. Cheng, W. Lu, L. Wang, X. Zhang, The bone tissue compatibility of a new Ti35Nb2Ta3Zr alloy with a low Young's modulus, Int. J. Mol. Med. 31 (2013) 689-697.
57. J. Li, S.J. Li, Y.L. Hao, H.H. Huang, Y. Bai, Y.Q. Hao, Z. Guo, J.Q. Xue, R. Yang, Electrochemical and surface analyses of nanostructured Ti–24Nb–4Zr–8Sn alloys in simulated body solution, Acta Biomater. 10 (2014) 2866-2875.
58. K.C. Nune, R.D.K. Misra, S.J. Li, Y.L. Hao, R. Yang, Osteoblast cellular activity on low elastic modulus Ti–24Nb–4Zr–8Sn alloy, Dental Mater. 33 (2017) 152-165.
59. S. Bălțatu, P. Vizureanu, D. Mareci, L.C. Burtan, C. Chiruță, L.C. Trincă, Effect of Ta on the electrochemical behavior of new TiMoZrTa alloys in artificial physiological solution simulating in vitro inflammatory conditions, Mater. Corros.67 (2016) 1314-1320.
60. M.S. Bălțatu, P. Vizureanu, V. Geantă, C. Nejneru, C.A. Țugui, S.C. Focşăneanu, Obtaining and mechanical properties of Ti-Mo-Zr-Ta alloys, IOP Conf. Series: Mater. Sci. Eng. 209 (2017) 012019. doi:10.1088/1757-899X/209/1/012019.
61. M.S. Bălțatu, P. Vizureanu, T. Bălan, M. Lohan, C.A. Țugui, Preliminary tests for Ti-Mo-Zr-Ta alloys as potential biomaterials, IOP Conf. Series: Mater. Sci. Eng. 374 (2018) 012023. doi:10.1088/1757-899X/374/1/012023.
62. ASTM F 2066, Standard specification for wrought titanium-15 molybdenum alloy for surgical implant applications (UNS R58150), ASTM International, West Conshohocken, PA, 2011.
63. G. Bolat, D. Mareci, R. Chelariu, J. Izquierdo, S. González, R.M. Souto, Investigation of the electrochemical behaviour of TiMo alloys in simulated physiological solutions, Electrochim. Acta 113 (2013) 470–480.

64. R.W. Schutz, An overview of beta titanium alloy environmental behavior, in: Beta Titanium Alloys in the 1990's, D. Eylon, R. Boyer, D.A. Koss (Eds.), The Minerals, Metals & Materials Society, Warrendale, PA, 1993, pp. 75-91.
65. G. Bolat, J. Izquierdo, T. Gloriant, G. Bolat, J. Izquierdo, T. Gloriant, R. Chelariu, D. Mareci, R.M. Souto, Investigation of processing effects on the corrosion resistance of Ti20Mo alloy in saline solutions, Corros. Sci. 98 (2015) 170-179.
66. L.C. Zhang, T. Zhou, M. Aindow, S.P. Alpay, M.G. Blackburn, Nucleation of stress-induced martensites in a Ti/Mo-based alloy, J. Mater. Sci. 40 (2005) 2833-2836.
67. C.J. Frandsen, K.S. Brammer, K. Noh, G. Johnston, S. Jin, Tantalum coating on TiO_2 nanotubes induces superior rate of matrix mineralization and osteofunctionality in human osteoblasts. Mater. Sci. Eng. C 37 (2014) 332-341.
68. Q. Wang, Y. Qiao, M. Cheng, G. Jiang, G. He, Y. Chen, X. Zhang, X. Liu, Tantalum implanted entangled porous titanium promotes surface osseointegration and bone ingrowth, Sci. Rep. 6 (2016) 26248, 13 pp. doi:10.1038/srep26248.
69. T.R. Arnett, Acid–base regulation of bone metabolism, Int. Congr. Ser. 1297 (2007) 255-267. doi:10.1016/j.ics.2006.08.005.
70. J. Malda, T.J. Klein, Z. Upton, The roles of hypoxia in the in vitro engineering of tissues, Tissue Eng. 13 (2007) 2153-2162.
71. ISO 10993-2:2006/(R) 2010, Biological evaluation of medical devices—Part 2: Animal welfare requirements. ISO Geneva, 2010.
72. M. Fântânariu , L.C. Trincă, C. Solcan, A.E. Trofin, Ş. Strungaru, E. Şindilar, G. Plăvan, S. Stanciu, A new Fe-Mn-Si alloplastic biomaterial as bone grafting material: In vivo study, Appl. Surf. Sci. 352 (2015) 129–139.
73. L.C. Trincă, M. Fântânariu, C. Solcan, A.E. Trofin, L. Burtan, D.M. Acatrinei, S. Stanciu, B. Istrate, C. Munteanu, In vivo degradation behavior and biological activity of some new Mg–Ca alloys with concentration's gradient of Si for bone grafts, Appl. Surf. Sci. 352 (2015) 140–150.
74. J.A. Kiernan, Histological and Histochemical Methods: Theory and Practice, 4th edn., Scion Publishing Ltd, Bloxham, UK, 2008.
75. A.C. Allori, A.M. Sailon, S.M. Warren, Biological basis of bone formation, remodeling, and repair-part II: Extracellular matrix, Tissue Eng. Part B Rev. 14 (2008) 273-285.
76. E. Takeda, Y. Taketani, N. Sawada, T. Sato, H. Yamamoto, The regulation and function of phosphate in the human body, Biofactors 21 (2004) 345-355.

77. S. Khoshniat, A. Bourgine, M. Julien, P. Weiss, J. Guicheux, L. Beck, The emergence of phosphate as a specific signaling molecule in bone and other cell types in mammals, Cell. Mol. Life Sci. 68 (2011) 205-218.
78. A. Komnenou, M. Karayannopoulou, Z.S. Polizopoulou, T.C. Constantinidis, A. Dessiris, Correlation of serum alkaline phosphatase activity with the healing process of long bone fractures in dogs, Vet. Clin. Path. 34 (2005) 35–38.
79. H. Orimo, The mechanism of mineralization and the role of alkaline phosphatase in health and disease, J. Nippon Med. Sch. 77 (2010) 4-12.
80. E.E. Golub, B.B. Kathleen, The role of alkaline phosphatase in mineralization, Curr. Opin. Orthop. 18 (2007) 444–448.
81. A. Roshan-Ghias, A. Vogel, L. Rakotomanana, D.P. Pioletti, Prediction of spatio-temporal bone formation in scaffold by diffusion equation, Biomaterials 32 (2011) 7006-7012.
82. J. Chou, J. Hao, S. Kuroda, D. Bishop, B. Ben-Nissan, B. Milthorpe, M. Otsuka, Bone regeneration of rat tibial defect by zinc-tricalcium phosphate (Zn-TCP) synthesized from porous Foraminifera carbonate macrospheres, Mar. Drugs 11 (2013) 5148-5158.
83. Y. Qiao, W. Zhang, P. Tian, F. Meng, H. Zhu, X. Jiang, L. Xiu, P.K. Chu, Stimulation of bone growth following zinc incorporation into biomaterials, Biomaterials 35 (2014) 6882-6897.
84. E.P.M. van Westing, G.M. Ferrari, J.H.W. de Wit, The determination of coating performance with impedance measurements - I. Coating polymer properties, Corros. Sci. 34 (1993) 1511-1530.
85. G. Rondelli, B. Vicentini, Effect of copper on the localized corrosion resistance of Ni-Ti shape memory alloy, Biomaterials 23 (2002) 639-644.
86. Y.S. Amin, J. van der Stok, Y.C. Chai, R. Wauthle, B.Z. Tahmasebi, P. Habibovic, M. Mulier, J. Schrooten, H. Weinans, A.A. Zadpoor, Bone regeneration performance of surface-treated porous titanium, Biomaterials 35 (2014) 6172-6181.
87. D. Miao, A. Scutt, Histochemical localization of alkaline phosphatase activity in decalcified bone and cartilage, J. Histochem. Cytochem. 50 (2002) 333-340.

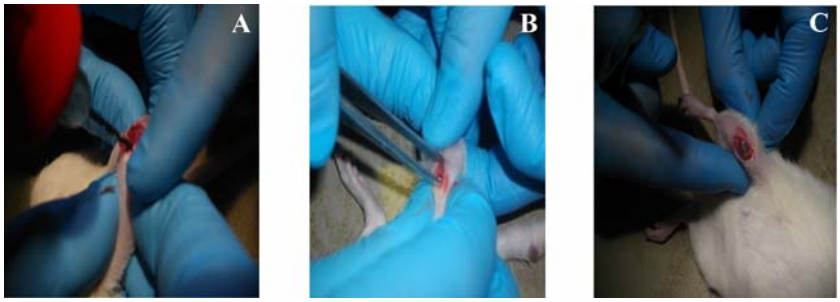

Figure 1. Main surgical stages followed for the tibiae implantation in Sprague–Dawley rats.

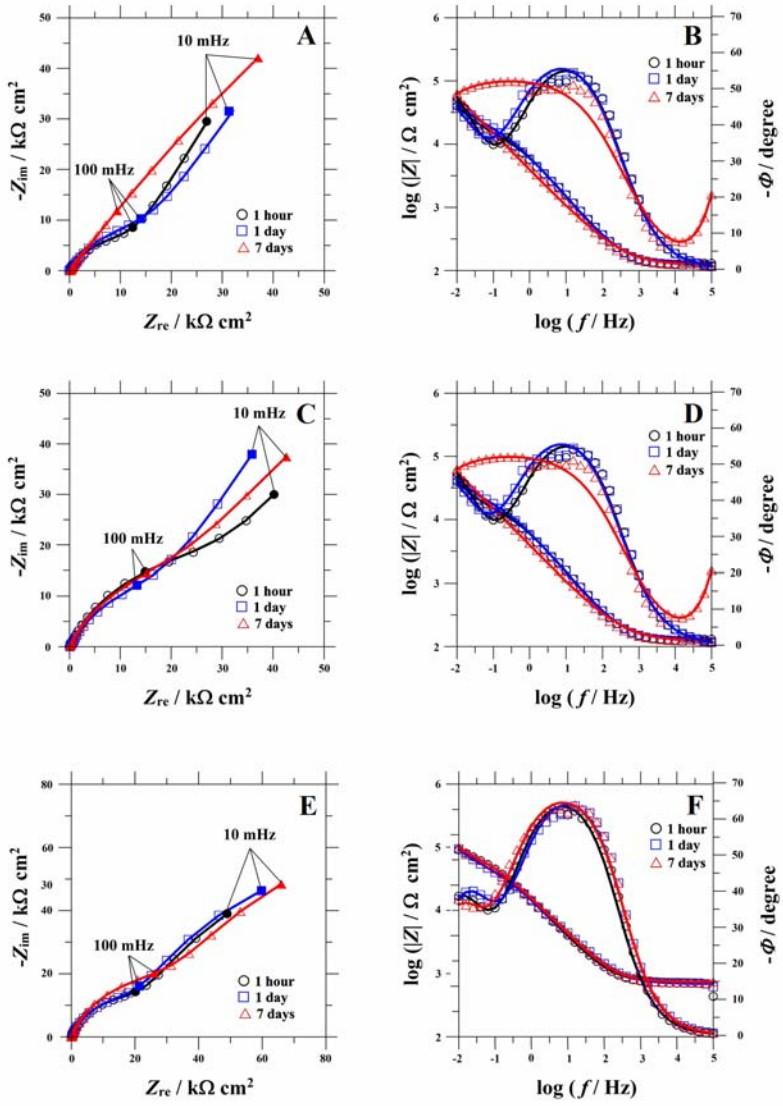

Figure 2. (A,C,E) Nyquist and (B,D,F) Bode plots for the quaternary TiMoZrTa alloys immersed in aerated acidified simulated physiological solution at 37 ^{o}C for different immersion times. The solid lines and the discrete points correspond to the fitted and the measured data, respectively. (A,B) Ti-20Mo-7Zr-5Ta, (C,D) Ti-20Mo-7Zr-10Ta, and (E,F) Ti-20Mo-7Zr-15Ta.

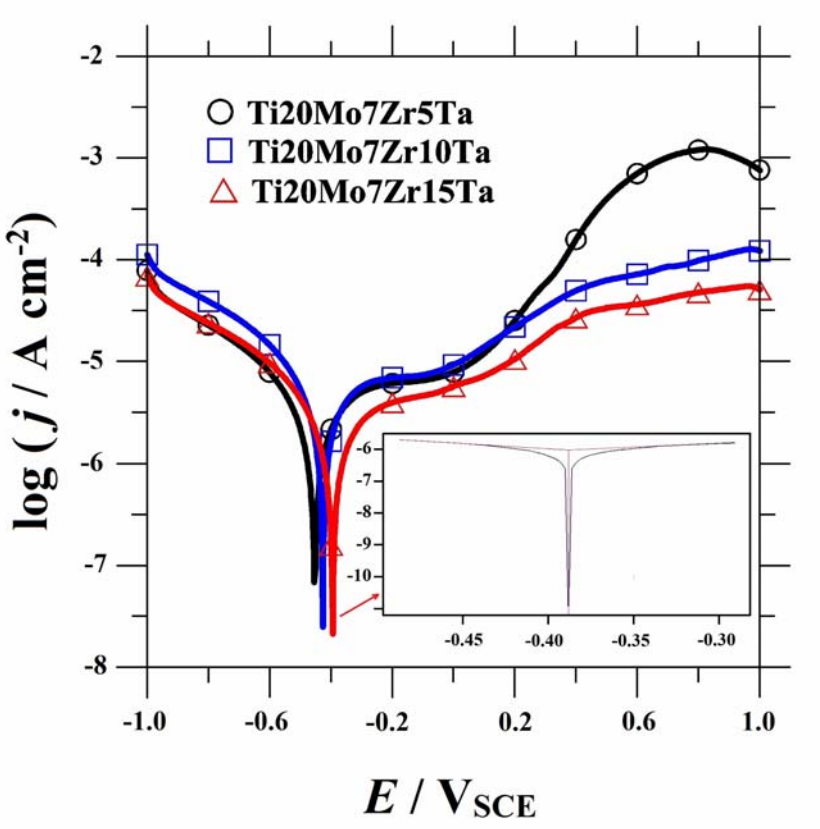

Figure 3. Linear potentiodynamic polarization curves measured for the quaternary TiMoZrTa alloys after 7 days immersion in acidified simulated physiological solution at 37 ^{o}C. The inset shows the application of Tafel analysis to the LPP data measured for Ti-20Mo-7Zr-15Ta alloy.

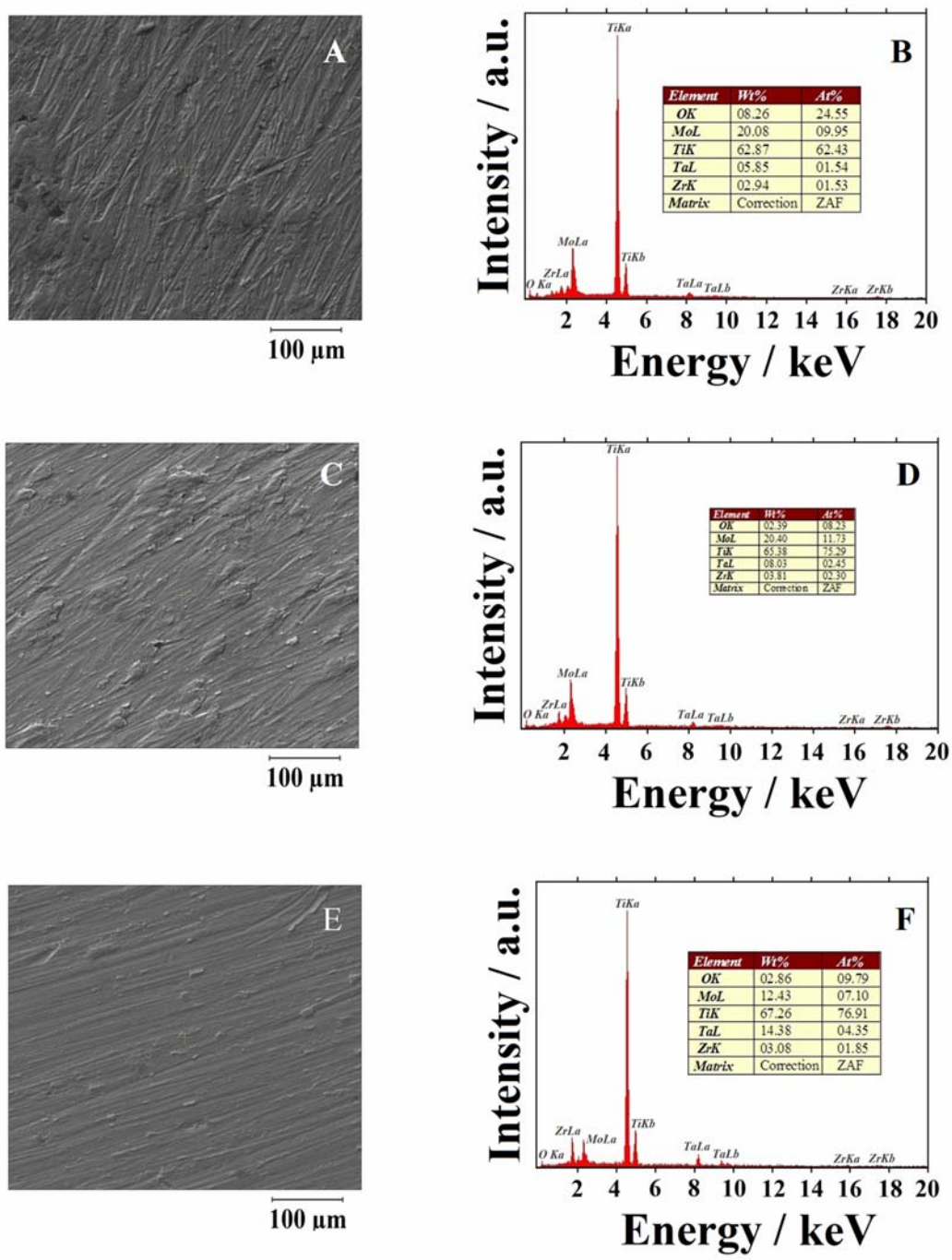

Figure 4. Representative (A,C,E) SEM and corresponding (B,D,F) EDX observations of quaternary TiMoZrTa alloys retrieved at +1.0 V_{SCE} from acidified simulated physiological solution at 37 ^{o}C after completing the linear potentiodynamic polarization tests. Alloys: (A,B) Ti-20Mo-7Zr-5Ta, (C,D) Ti-20Mo-7Zr-10Ta, and (E,F) Ti-20Mo-7Zr-15Ta.

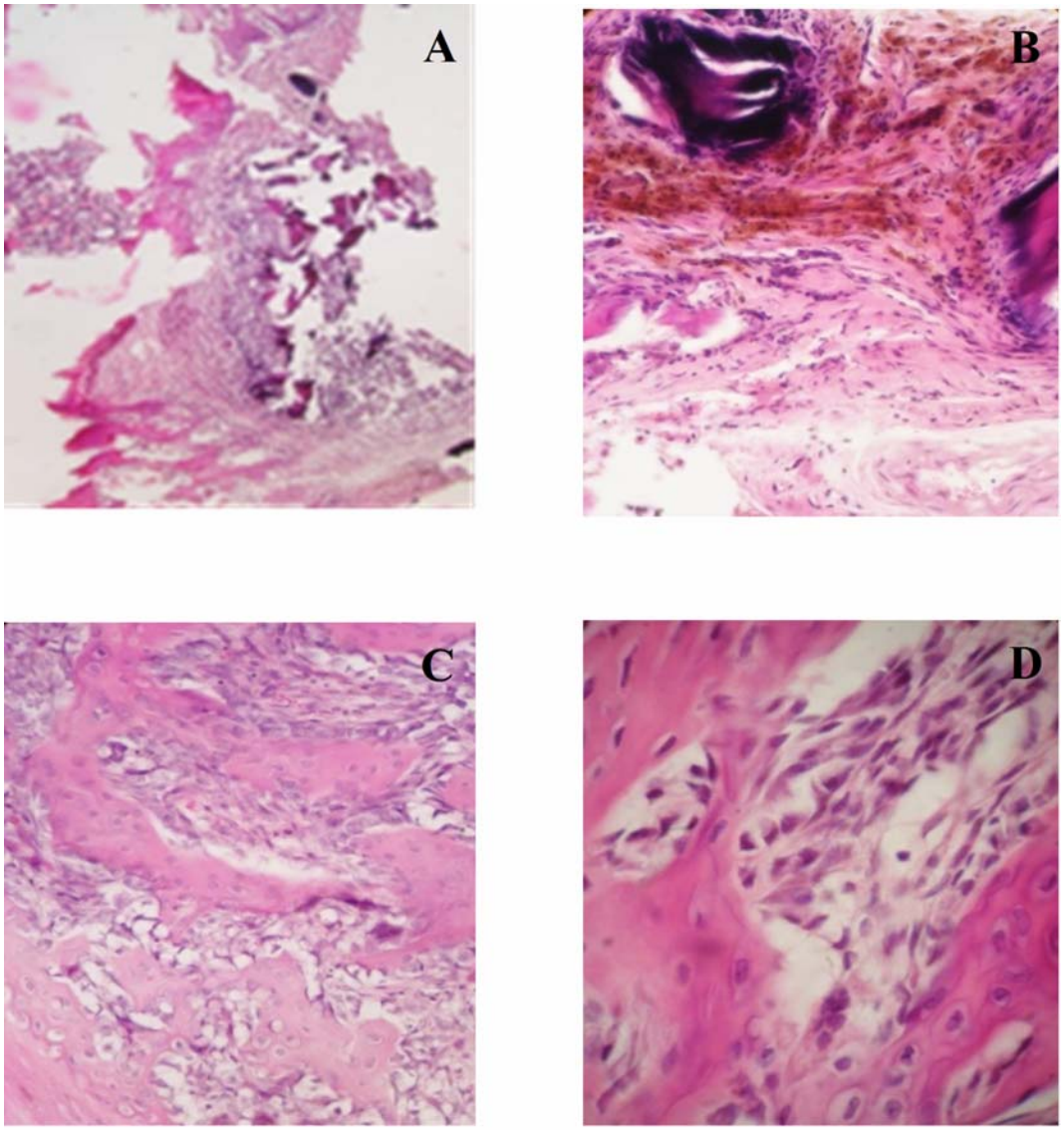

Figure 5. Hystology sections of osseous tissue at (A,B) 14 and (C,D) 28 days implantation in a rat from G1 group (with Ti-20Mo-7Zr-5Ta alloy implant). (A) Bone necrosis (HE stain, ×60); (B) peripheral ongoing repairing process (PAS stain, ×100); (C) osteoid tissue surrounded by a fibrous background (PAS stain, ×200); (D) osteocyte lacunae (with bigger staining affinity) in the remodeled area (PAS stain, ×900).

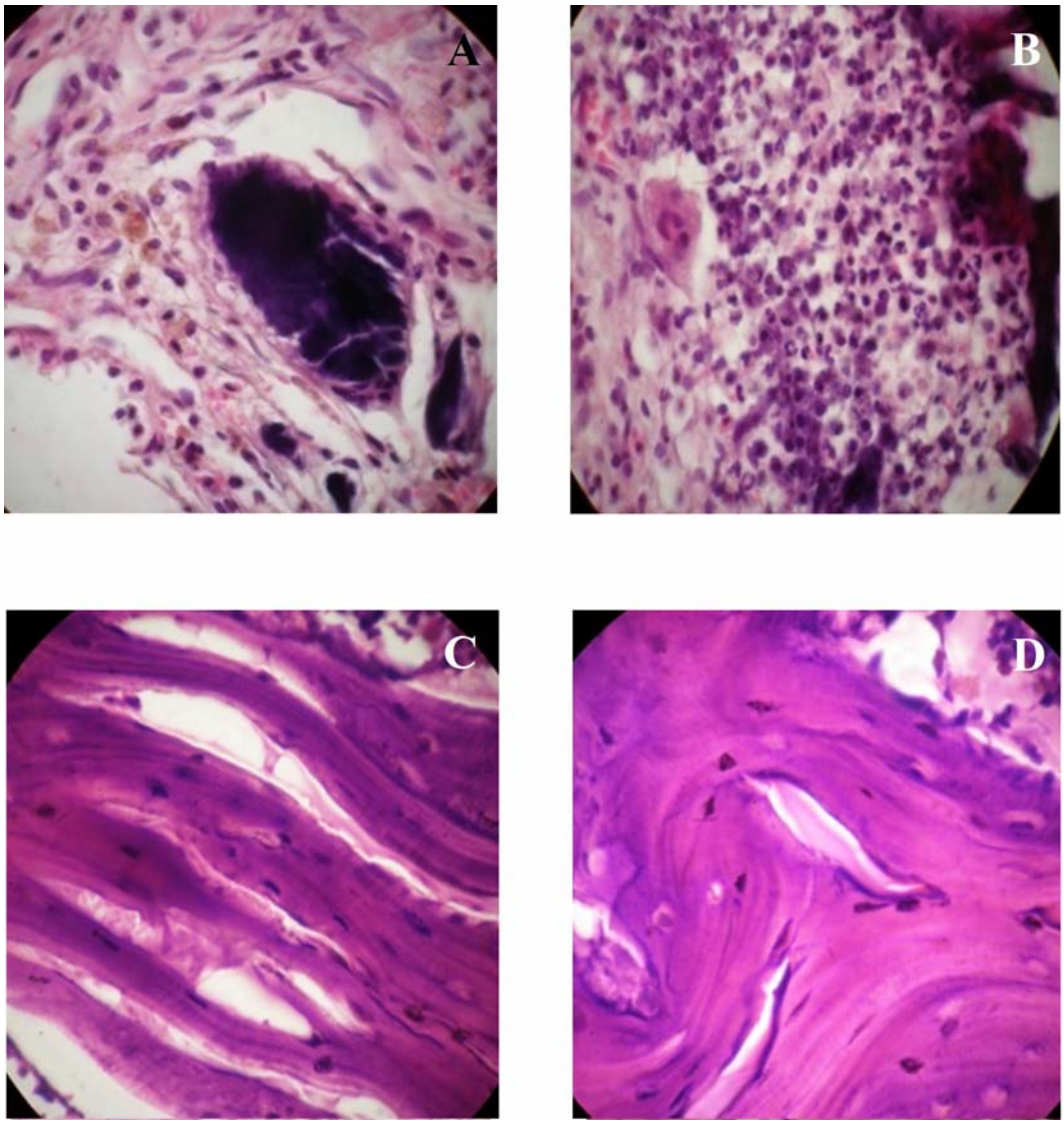

Figure 6. Hystology sections of osseous tissue at (A,B) 14 and (C,D) 28 days implantation in a rat from G2 group (with Ti-20Mo-7Zr-15Ta alloy implant). (A) Bony necrotic area (dark violet) surrounded by numerous macrophages with brown phagocytized wear pigments (HE stain, ×900); (B) fibrous connective tissue, with mono- and polymorphonuclear inflammatory infiltrate (HE stain, ×400); (C) newly bone tissue with a rocklike roughened surface (HE stain, ×400); D) mini-remodelation of the new osseous matrix (HE stain, ×900).

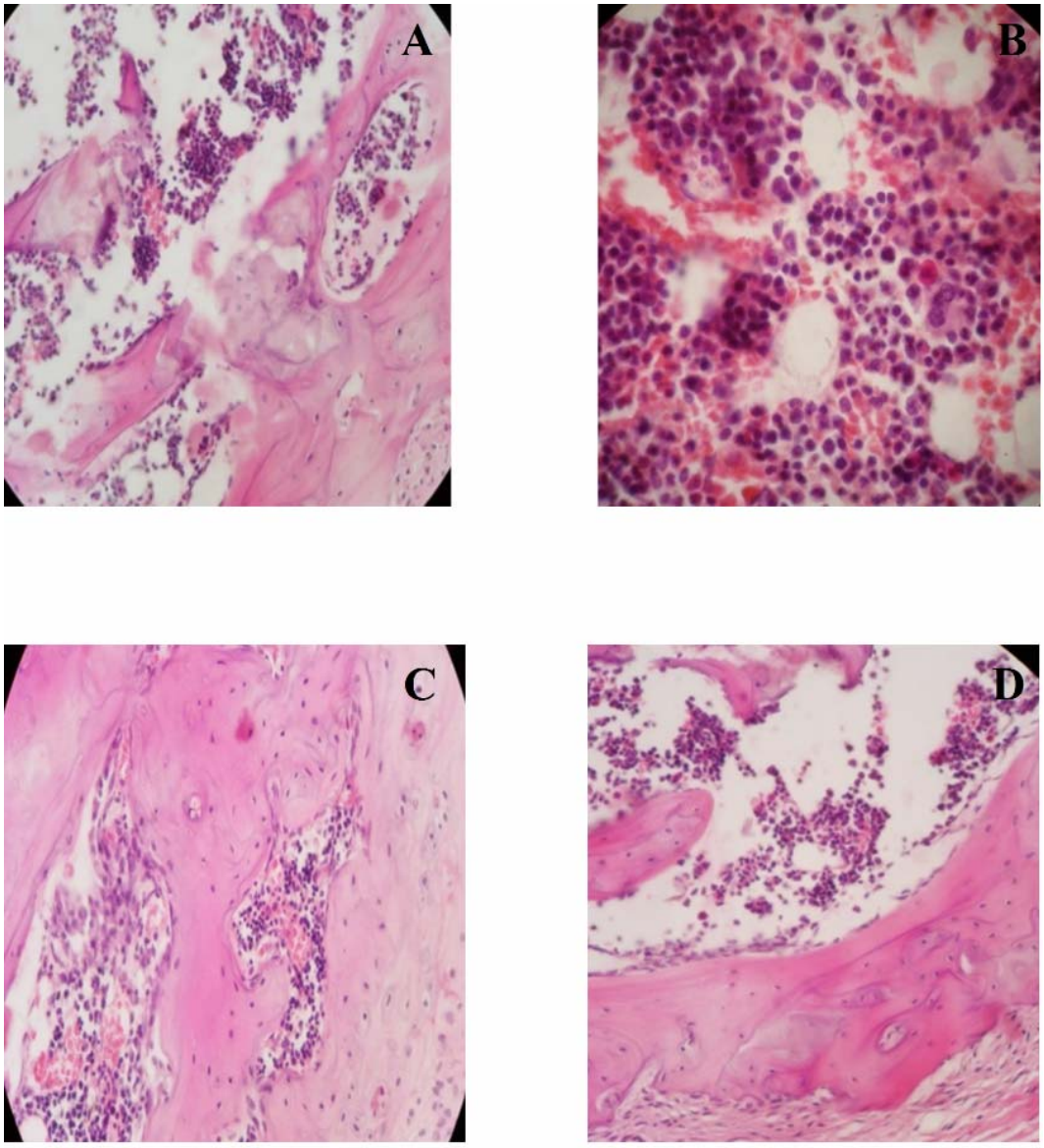

Figure 7. Hystology sections of osseous tissue at (A,B) 14 and (C,D) 28 days implantation in a rat from G2 group (with Ti-20Mo-7Zr-15Ta alloy implant). (A) Bony necrotic area (HE stain, ×100); (B) blood cells in bone marrow (HE stain, ×100); (C) osteoblasts (lighter coloured areas) synthesizing the collagen matrix I (HE stain, ×400); D) osteoclasts and nucleated osteocytes (HE stain, ×400).

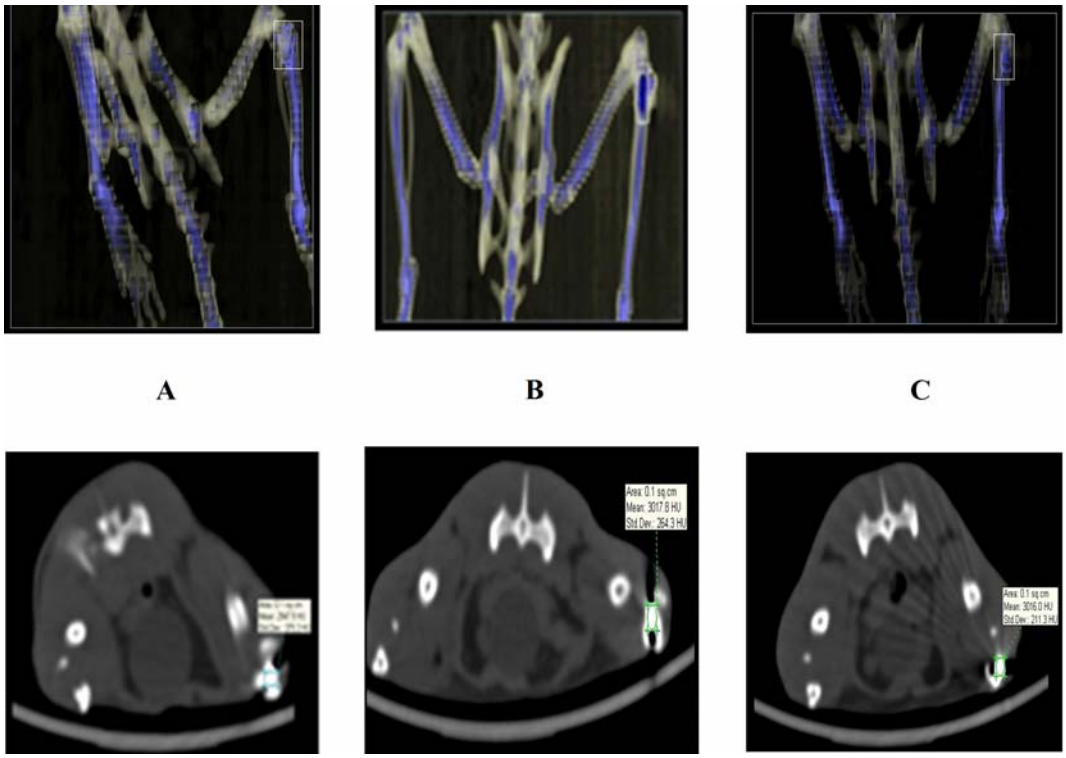

Figure 8. 3D&2D reconstructed images of computed tomography (CT) analysis. Implant group: (A) in a rat from group G1 (with Ti-20Mo-7Zr-5Ta alloy implant); B) in a rat from group G2 (with Ti-20Mo-7Zr-15Ta alloy implant); and (C) in a rat from group G3 (with cp-Ti implant).

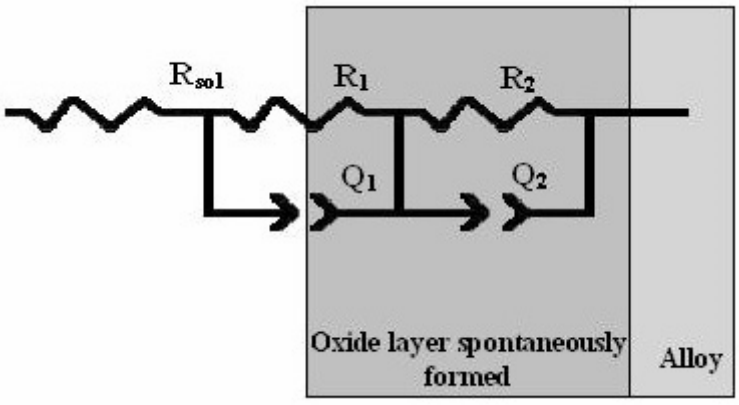

Figure 9. Equivalent circuit (EC) used for the interpretation of the measured impedance spectra.

Table 1. Chemical compositions (wt.%) and "molybdenum equivalent" [Mo_{eq}] [64] of the quaternary TiMoZrTa alloys.

Alloy	Composition / wt.%	[Mo_{eq}]
Ti-20Mo-7Zr-5Ta	Ti-19.8-Mo%-6.8Zr%-4.9%Ta	21.1
Ti-20Mo-7Zr-10Ta	Ti-20.2-Mo%-6.7Zr%-9.9%Ta	22.2
Ti-20Mo-7Zr-15Ta	Ti-20.4-Mo%-7.1Zr%-.14.8%Ta	23.3

Table 2. Mean and standard deviation values of main electrochemical parameters determined from potentiodynamic polarization curves for quaternary TiMoZrTa alloys after 7 days immersion in acidified simulated physiological solution.

Alloy	ZCP / V_{SCE}	$-\beta_c$ / V decade^{-1}	β_a / V decade^{-1}	j_{cor} / µA cm^{-2}	j_{pas}* / µA cm^{-2}
Ti-20Mo-7Zr-5Ta	-0.454 (0.026)	0.151 (0.011)	0.199 (0.014)	1.8 (0.6)	54 (8)
Ti-20Mo-7Zr-10Ta	-0.425 (0.021)	0.156 (0.010)	0.191 (0.012)	1.2 (0.4)	32 (4)
Ti-20Mo-7Zr-15Ta	-0.388 (0.017)	0.149 (0.010)	0.189 (0.011)	0.8 (0.3)	18 (2)

*Values determined at +0.3 V_{SCE}

Table 3. Biochemical markers determined from the blood serum in rats without and with bone (tibiae) implant.

Parameter	Control group	Experimental Group / Implant material					
		G1 / Ti-20Mo-7Zr-5Ta alloy		G2 / Ti-20Mo-7Zr-5Ta alloy		G3 / Cp-Ti	
		14th day	28th day	14th day	28th day	14th day	28th day
Ca / mg dL^{-1}	11.56 ± 0.897	9.22 ± 0.932	10.86 ± 0.924	9.11 ± 0.101	11.44 ± 0.888	9.44 ± 0.991	11.32 ± 0.952
Inorganic Phosphate / mg dL^{-1}	10.11 ± 0.920	7.23 ± 0.634	8.84 ± 0.821	8.0 3 ± 0.762	9.78 ± 0.820	7.65 ± 0.533	8.66 ± 0.915
(ALKP/TP) / U g^{-1}	1.34 ± 0.164	1.84 ± 0.770	1.44 ± 0.160	1.99 ± 0.188	1.39 ± 0.138	1.86 ± 0.202	1.52 ± 0.166

Table 4. Electrochemical parameters extracted from impedance spectra through modelling experimental data for quaternary TiMoZrTa alloys in acidified simulated physiological solution after different immersion times to the equivalent circuit containing two time constants shown in Figure 9.

Alloy	Immersion time	Q_1 / mS cm^{-2} s^n	n_1	R_1 / kΩ cm^2	Q_2 / μS cm^{-2} s^n	n_2	R_2 / kΩ cm^2
Ti-20Mo-7Zr-5Ta	1 hour	17	0.80	1.6	0.22	0.81	42
	1 day	17	0.81	1.8	0.22	0.81	46
	7 days	16	0.82	1.9	0.21	0.82	54
Ti-20Mo-7Zr-10Ta	1 hour	15	0.81	3.1	0.21	0.82	51
	1 day	15	0.81	3.4	0.21	0.82	55
	7 days	15	0.82	3.9	0.19	0.83	61
Ti-20Mo-7Zr-15Ta	1 hour	12	0.81	6.7	0.19	0.83	63
	1 day	12	0.82	7.1	0.17	0.83	78
	7 days	11	0.82	7.8	0.16	0.83	85